

CHALMERS
UNIVERSITY OF TECHNOLOGY

Digital Control Implementation for Coupling Independent IPT Systems without Communication

Downloaded from: https://research.chalmers.se, 2026-11-24 23:25 UTC

Citation for the original published paper (version of record):
Lai, L., Huang, J., Tang, J. et al (2024). Digital Control Implementation for Coupling Independent IPT Systems without Communication. 2024 IEEE 10th International Power Electronics and Motion Control Conference, IPEMC 2024 ECCE Asia: 3350-3356.
http://dx.doi.org/10.1109/IPEMC-ECCEAsia60879.2024.10567845

N.B. When citing this work, cite the original published paper.

© 2024 IEEE. Personal use of this material is permitted. Permission from IEEE must be obtained for all other uses, in any current or future media, including reprinting/republishing this material for advertising or promotional purposes, or reuse of any copyrighted component of this work in other works.

(article starts on next page)

Digital Control Implementation for Coupling Independent IPT Systems without Communication

Linhua Lai[1]*, Jiasheng Huang[2]*, Junfei Tang[1], Ziwei Ouyang[2], Yujing Liu[1], and Michael A.E. Andersen [2]
[1]Department of Electrical Engineering, Chalmers University of Technology, 412 96 Göteborg, Sweden
[2] Department of Electrical and Photonics Engineering, Technical University of Denmark, 2800 Kgs. Lyngby, Denmark
* Equal contribution for this paper
Email: linhua@student.chalmers.se; jiahuan@dtu.dk; junfei.tang@chalmers.se;
ziou@dtu.dk; yujing.liu@chalmers.se; maea@dtu.dk

***Abstract*—Inductive Power Transfer (IPT) offers a convenient solution for charging electric vehicles (EVs). By synchronizing the inverter output voltage with current, a parity-time (PT)-symmetric IPT system can operate in the PT-symmetric mode, ensuring that the transfer power and efficiency remain independent of misalignment. However, the inherent propagation delay in the control circuit can lead to synchronization failure, reducing the efficiency of the system. In this article, the influence of propagation delay are analyzed. The results show that propagation delay increases the switching loss of system, causes working frequency and output power drift. To address this issue, a novel digital control scheme is proposed to compensate for propagation delay without requiring any extra component. The theoretical analysis and the feasibility of the compensation control scheme are validated through experiments with an IPT prototype. The results show that the maximum efficiency can be achieved when the system is slightly over-compensated. Within a misalignment range of 0-160 mm, the fully-compensated system maintains nearly constant output power.**

***Index Terms*—Inductive power transfer (IPT), Parity-time (PT)-symmetric circuit, Misalignment tolerance, Propagation delay**

I. Introduction

Inductive Power Transfer (IPT) has been widely studied over the past 30 years due to the convenience and safety that it has offered to charge electric vehicles (EVs) [1]–[3]. In previous research, the coupled magnetic resonant circuit has been the most extensively investigated structure for building IPT systems [4], [5]. In conventional IPT systems, the output power and efficiency are sensitive to the coupling that exists between the coils [6], which is determined by the type and misalignment of the coils. In practice, the misalignment depends on the parking position of EVs. This poses a challenge for building an IPT system that provides a constant output power regardless of misalignment variation.

In previous works, many approaches have been proposed to enhance the misalignment tolerance of IPT systems. These approaches can be categorized into two aspects, 1) to optimize magnetic coupler design [7], [8], [8]–[10] and 2) to employ control strategies [11], [12]. In [9], a 6.78 MHz 200 W IPT system is built with an optimized coupler design. An analytical model-based optimization method is applied to obtain a magnetic coupler with high misalignment tolerance and efficiency. Additionally, Zhi Bie et al. [13] propose an asymmetric magnetic coupler design utilizing the horizontal magnetic field of the transmitter coil for unmanned aerial vehicle applications. This structure shows advantages of free-rotation and offset tolerance. The stray field around a 3.3 kW IPT charger is analyzed in [14], and the result shows that the requirement on leakage flux density can be fulfilled easily for a low-power IPT charger. However, it's worth noting that asymmetrically designed coils may become space and material-consuming in high-power IPT charging scenarios.

Utilizing control strategies to improve misalignment tolerance becomes a cost-effective solution for high-power applications. In [15], the author proposes an IPT system based on magnetic in-band communication. The information is transmitted to the transmitter side through low-frequency voltage component. To further boost system efficiency, Chao Cui et al. investigate the ZVS operating range of a DAB IPT system [16]. The results show that soft switching can be achieved by adjusting the bilateral load angle. A back-to-back connected prototype is established in [17] with synchronous rectification on the receiver side. This configuration achieves a transmission power of 45.9 kW with a system efficiency of 96.6%. However, the efficiency and output power of the system are highly impacted by the coupling condition. To achieve output power independence of coupling variations, an IPT system based on a PT-symmetric circuit is proposed in [18]. In this approach, the power source is treated as a negative resistor, enabling constant output power and efficiency in strong coupling regions, irrespective of the coupling coefficient variation. Moreover, this control scheme relies solely on the transmitter current, eliminating the need for wireless communication. In [19], the stability and steady-state working frequency of PT-symmetric circuit are discussed. The control strategy fulfilling the negative resistance source is further explored in [20], where a synchronization circuit is employed to control the phase angle between the inverter output voltage and current. The proposed control scheme requires high-speed controllers and amplifiers to mitigate the influence of inherent propagation delay, which exists in the control circuit. Consequently, this increases the

complexity and cost of the control system. Besides, the propagation delay causes a hard-switching problem, which reduces the efficiency of the system. However, neither discussion on the effect of propagation delay nor the compensation method has been analyzed. Therefore, to improve the robustness of IPT system while keeping high efficiency, study on a control scheme taking delay into consideration is necessary.

The rest of this article is organized as follows: the system structure and ideal model are provided in Section II. The influence of the propagation delay is analyzed and a digital compensation scheme is proposed in Section III. To verify the analysis and the effect of compensation scheme, an IPT prototype is introduced and the experimental results are shown in Section IV. Finally, conclusions are given in Section V.

II. IPT System Configuration and Ideal Model

A. Ideal Circuit Model

A schematic of the setup of the system is shown in Fig. 1a. The system comprises a DC voltage source, a full-bridge inverter, a controller, coupled transmitter and receiver coils, series-series(S-S) compensation, a diode rectifier, and the load. The inverter transforms dc voltage V_{dc} to square voltage v_{in}. i_1 and i_2 are currents in the transmitter and receiver coils, respectively. V_o is the load voltage and R_L is the load. Considering the fundamental components of voltage and current, the equivalent circuit can be obtained as shown in Fig. 1b. The following relationship holds for the input and output

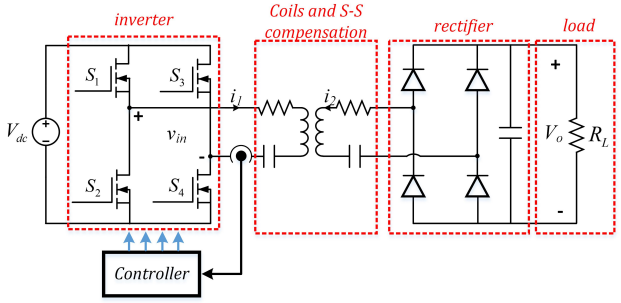

(a) IPT system configuration

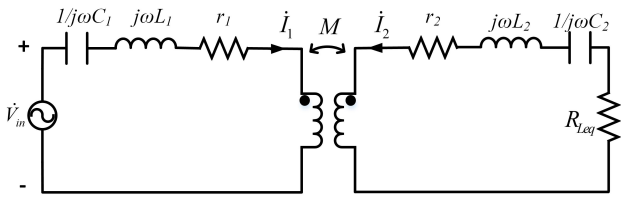

(b) Equivalent circuit

Fig. 1: System configuration and equivalent circuit

of the inverter and rectifier.

$$\begin{cases} V_{in} = 2\sqrt{2}V_{dc}\sin(D\pi)/\pi, R_{Leq} = 8R_L/\pi^2 \\ Z_{in} = \dot{V}_{in}/\dot{I}_1 = R_n + jX_n \end{cases} \tag{1}$$

In the equivalent circuit, ω is the switching angular frequency, L_1 and L_2 are the self-inductance of the transmitter and receiver coils, respectively. C_1 and C_2 are compensation capacitances. r_1 and r_2 are equivalent series resistances. k is coupling factor, $M = k\sqrt{L_1 L_2}$ is mutual inductance, D is the duty cycle of the inverter, V_{in} is the RMS value of $\dot{V}_{in}$, Z_{in} is the input impedance. According to the circuit theorem, the equivalent input impedance of the system can be described as follows:

$$\begin{cases} R_n = r_1 + \dfrac{(\omega M)^2(R_{Leq}+r_2)}{(R_{Leq}+r_2)^2 + (\omega L_2 - \frac{1}{\omega C_2})^2} \\ X_n = \omega L_1 - \dfrac{1}{\omega C_1} - \dfrac{(\omega M)^2(\omega L_2 - \frac{1}{\omega C_2})}{(R_{Leq}+r_2)^2 + (\omega L_2 - \frac{1}{\omega C_2})^2} \end{cases} \tag{2}$$

According to the PT-symmetric condition, the inverter output voltage is synchronized with transmitter current. The input power source is regarded as a negative resistance [18]. In other words, the system has a unity input power factor ($X_n = 0$). Considering the case that the system has matched resonance frequency (i.e., $\sqrt{L_1C_1} = \sqrt{L_2C_2} = 1/\omega_0$), then the following relationship can be deduced from (2):

$$\frac{L_1}{L_2} = \frac{(\omega M)^2}{(R_{Leq}+r_2)^2 + (\omega L_2 - \frac{1}{\omega C_2})^2} \tag{3}$$

By solving (3), the working frequency ω can be obtained as follows:

$$\begin{cases} \omega = \omega_0 & k \le k_c \\ \omega = \omega_{l,h,0} & k > k_c \end{cases} \tag{4}$$

where

$$\begin{cases} \omega_{l,h} = \sqrt{\dfrac{-(\Gamma_2^2 - 2\omega_0^2) \pm \sqrt{\Delta}}{2(1-k^2)}} \\ \Delta = -4\omega_0^2\Gamma_2^2 + \Gamma_2^4 + 4k^2\omega_0^4 \\ \Gamma_2 = \dfrac{R_{Leq}+r_2}{L_2}, k_c = \dfrac{\Gamma_2}{\omega_0^2}\sqrt{\omega_0^2 - \dfrac{\Gamma_2^2}{4}} \end{cases} \tag{5}$$

Therefore, the working conditions can be separated into two regions based on the coupling factor.

When $k > k_c$, the system works in the PT-symmetric region. The system can work in either ω_l or ω_h. When the system works in PT-symmetric region with working frequency $\omega_{l,h}$, the output power and efficiency can be calculated as:

$$\begin{cases} P_{out} = \dfrac{R_{Leq}V_{in}^2}{\frac{L_1}{L_2}(R_{Leq}+r_2)^2 + 2r_1(R_{Leq}+r_2) + \frac{L_2}{L_1}r_1^2} \\ \eta = \dfrac{R_{Leq}}{\frac{L_2}{L_1}r_1 + r_2 + R_{Leq}} \end{cases} \tag{6}$$

It has been demonstrated that in the PT-symmetric region, the transfer efficiency and transfer power are independent of the coupling factor [20]. The working frequency converges to either ω_h or ω_l when the negative resistance is achieved [18].

In cases where $k \le k_c$, the system works in broken PT-symmetric region with the working frequency $\omega = \omega_0$. The output power can be calculated as:

$$P_{out} = \frac{(\omega M V_{in})^2 R_{Leq}}{(r_1(r_2+R_{Leq}) + (\omega M)^2)^2} \tag{7}$$

It indicates that in the broken PT-symmetric region, the output power is subject to the coupling factor.

B. Soft Switching Analysis

When the switch is turned off, the D-S capacitance of the switch prevents the rapid voltage rising [21], [22]. Thus, the switches are regarded as soft switching off in this paper. Soft switching can be achieved using reactive current as the reverse current [22]. Considering a scenario with inverter duty cycle $D = 0.5$, Fig. 2 shows the waveform of inverter output voltage, output current, PWM signal, voltage and current across S_1 under the soft switching operation and hard switching operation. It can be observed that in the hard operation case, S_1 has turn-on loss because the inverter output voltage lags the current. On the other hand, in soft switching case, S_1 works in ZVS mode when turned on as the inverter output voltage leads the current. Similar analyses can be applied to other switches. It can be concluded that soft switching on can be realized when the inverter output voltage leads the current.

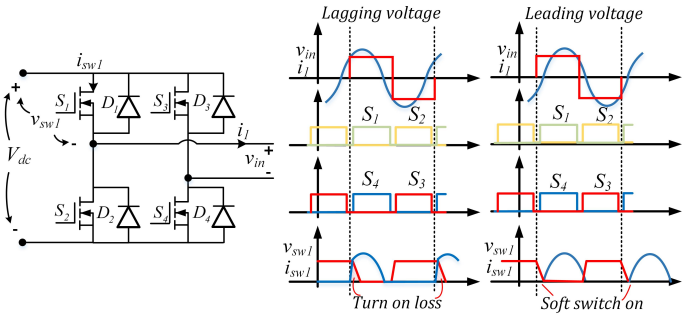

Fig. 2: The gate signals, inverter output voltage and transmitter current in inverter with soft switching and hard switching operation.

III. Influence of Delay and Digital Compensation Control Scheme

A. Influence of Delay and Compensation

To achieve PT-symmetric mode with unity input power factor, a phase synchronization method is necessary. Using a current sensor and zero-crossing comparator, the controller can sample the transmitter current and generate a gate signal that synchronizes with the current. However, the propagation delay in components of the control circuit can result in a lagging inverter output voltage, leading to synchronization failure and increasing the switching loss. This delay can significantly impact the performance of a digital control system. Considering a control system with propagation delay Δt_d, the phase difference between inverter output voltage $\dot{V}_{in}$ and transmitter current $\dot{I}_1$ is given by $\alpha = -\Delta t_d \omega$. The equivalent input reactance X_n in Fig. 1b becomes:

$$X_n = R_n tan(-\Delta t_d \omega) \tag{8}$$

By submitting (8) into (2), the working frequency ω and output power can be obtained as:

$$\begin{cases} \omega = f(\Delta t_d, k) \\ P_{out} = g(\Delta t_d, k) \end{cases} \tag{9}$$

This indicates that propagation delay leads to working frequency and output power drift. Therefore, to achieve a constant output power independence of coupling factor, a compensation is necessary to achieve PT-symmetric conditions. Considering a system with compensation Δt_c, the equivalent reactance becomes:

$$X_n = R_n \tan(-\Delta t \omega) \tag{10}$$

where $\Delta t = \Delta t_d - \Delta t_c$. Based on the phase difference between $\dot{V}_{in}$ and $\dot{I}_1$, there are three types of compensation shown in Fig. 3. In the fully-compensated case, where $\Delta t_d = \Delta t_c$, the voltage is synchronized with the current, resulting in the highest input power factor. In the under-compensated case, $\Delta t_d > \Delta t_c$, the propagation delay is not fully compensated, causing the voltage to lag behind the current. The power factor is lower than 1 and there exists a risk of hard switching. To achieve soft switching, an over-compensate method can be applied with $\Delta t_d < \Delta t_c$. The voltage leads current by an over-compensated angle. However, the over-compensated method reduces the input power factor and the circuit does not work in PT-symmetric conditions. Fig. 4 illustrates the

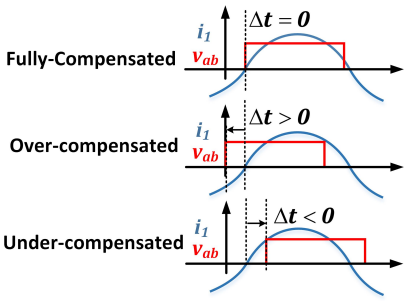

Fig. 3: Three types of compensation method

influence of under-compensation and over-compensation on frequency drift. The parameters selected for calculation are summarized in Table I. It can be found that when the voltage lags current for 300 ns, the working frequency is lower than the ideal PT-symmetric condition. Conversely, when the voltage leads the current by 300 ns, the working frequency is higher than the ideal PT-symmetric condition. This result indicates that propagation delay influences the working frequency of the circuit, emphasizing the necessity for compensation to achieve a PT-symmetric circuit.

B. Digital Compensation Control Scheme

Compensation is achieved through the digital control method illustrated in Fig. 5. Considering $D = 0.5$ as an example, v_{s1} is synchronized with v_{s4}. First, the current is measured by the Rogowski coil as i_{1m}. CTR is reset to 0 when DSP receives the rising zero crossing of i_{1m}. The current

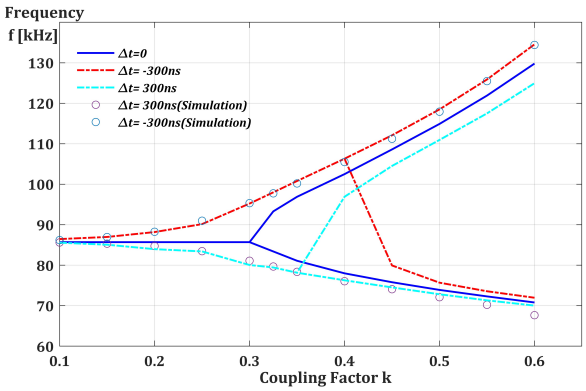

Fig. 4: Frequency drift due to delay and over-compensation

TABLE I: Parameter selection for frequency drift calculation

Parameter	Value	Parameter	Value
C_1	$47.14nF$	L_1	$73\mu H$
C_2	$47.14nF$	L_2	$73\mu H$
r_1	$69.8m\Omega$	r_2	$69.8m\Omega$
R_L	15Ω	k	$[0.1, 0.6]$

frequency can be calculated by measuring the time between two rising zero crossings. According to the latest measured current frequency, the switching frequency and the compare value CMPA and CMPB are updated. As shown in Fig. 5, v_{s1} is set when CTR reaches CMPA and cleared when CTR reaches CMPB. With $D = 0.5$, the comparable value CMPA and CMPB can be determined as follows:

$$\begin{cases} \text{CMPA} = \text{PRD} - \Delta t_c \\ \text{CMPB} = \text{CMPA} - \text{PRD}/2 \end{cases} \tag{11}$$

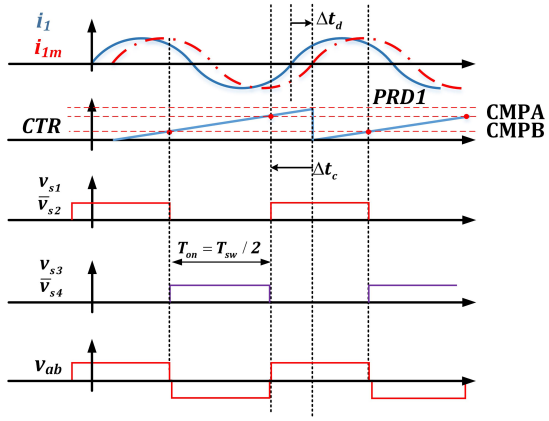

Fig. 5: Drive signal generation method based on compensation

The program flow chart is shown in Fig. 6. In this system, the working frequency is kept at low working frequency ω_l to reduce switching loss. The initial switching frequency $\omega_{init} = 70$ kHz. The maximum switching frequency is set to be $\omega_{max} = \omega_0 = 83.5$ kHz. As when measured current frequency $\omega > \omega_0$, the system is working in the broken PT-symmetric region and the only solution satisfying $X_n = 0$ is $\omega = \omega_0$. The minimum frequency $\omega_{min} = 60$ kHz to avoid runaway.

The compensation is accomplished through the digital control method, offering several advantages. The delay in the sample and control circuit can be effectively compensated through digital control to achieve a negative resistive source. This eliminates the need for additional compensation circuits and provides tunable compensation.

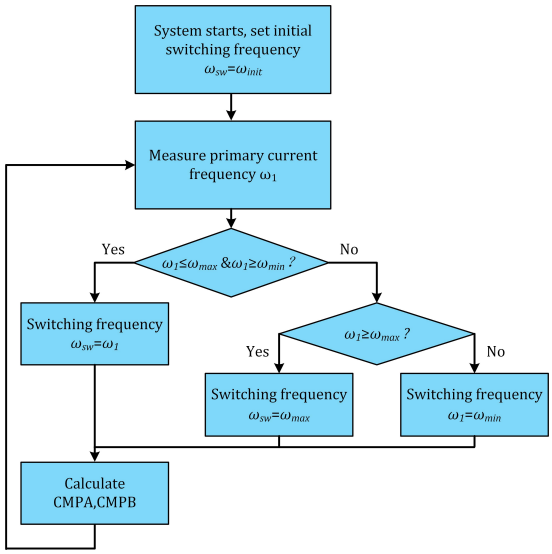

Fig. 6: Controller flow chart

IV. Experiment Validation and Analysis

A. Experimental Set Up

An IPT experiment system with digital control is built to verify the theoretical analysis. In this experiment, first, the effect of compensation and delay on system working frequency and efficiency is investigated. Subsequently, the horizontal misalignment d between coils is changed to study the performance of the PT-symmetric circuit in different compensation conditions. The experimental setup is illustrated in Fig. 7. A constant voltage source is connected to the input of the full bridge inverter, with the gate voltage provided by the CGD12HBXMP gate driver. The coils are designed as rectangular pads to fully utilize the available place (see Fig. 8). A constant resistance load is connected to the full bridge diode rectifier. The parameters and the dimension of coil are detailed in Table II. A synchronization circuit (see Fig. 9) is employed to synchronize the inverter output voltage with the current. A Rogowski coil is applied to measure the transmitter current. The rising zero crossing of current is captured by the amplifier and comparator. The zero crossing signal is then acquired by the DSP (TMS320F28379D), which generates PWM waves to control the gate driver. As the current zero crossing is the only signal being capture, there is no need of a high-speed sampling circuit. The total propagation delay in

the synchronization circuit consists of current sensor delay, amplifier delay, DSP delay, and driver delay, measuring a total of $\Delta t_d = 1800$ ns. This system has high misalignment tolerance when it operates in the PT-symmetric phase. Besides, soft switching can be achieved when the system works in the over-compensated mode.

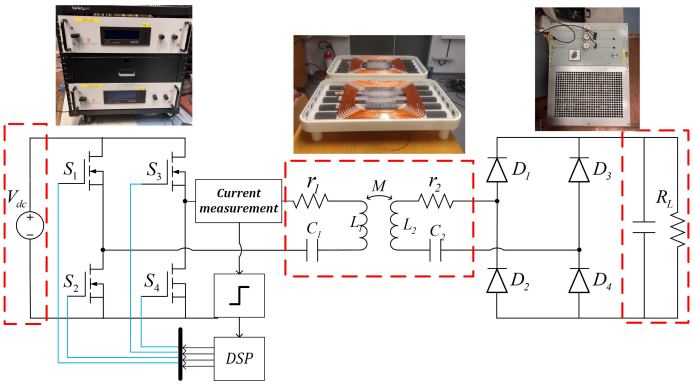

Fig. 7: Experimental set up

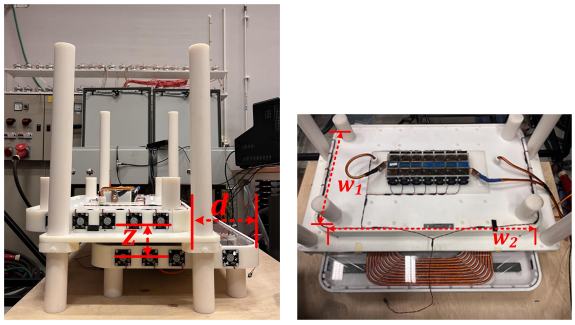

(a) Front view (b) Top view

Fig. 8: Coils for the experimental system

TABLE II: Parameter selection for experimental setup

Parameter	Value	Parameter	Value
C_1	45.80 nF	L_1	78.378 μH
C_2	45.204 nF	L_2	80.698 μH
r_1	147.10 $m\Omega$	r_2	133.62 $m\Omega$
Δt_c	$[0, 2500]$ ns	Δt_d	1800 ns
d	$[0, 250]$ mm	z	150 mm
R_L	16 Ω, 10 Ω	V_{dc}	200 V, 100 V
w_1	450 mm	w_2	740 mm

B. The Steady State Performance Under Different Compensations

The compensation Δt_c is varied to examine the effect of different compensations on the system's operation. The input DC voltage is set to $V_{dc} = 200$ V, and the load resistance is $R_L = 16\ \Omega$. The effect of compensation on frequency drift is shown in Fig. 10. It can be found that the working frequency increases with higher compensation. The system operates in a

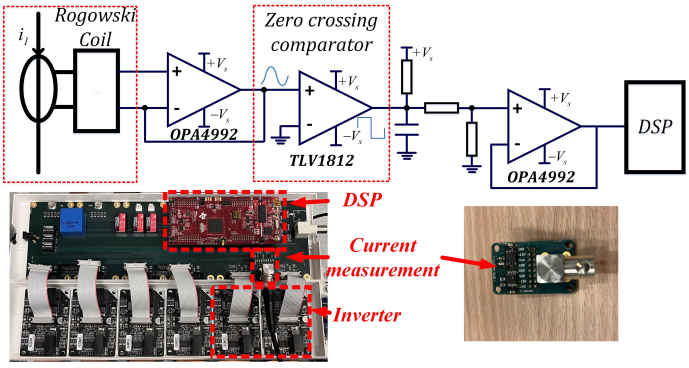

Fig. 9: Current sampling and synchronization circuit

PT-symmetric state when the propagation delay is fully compensated ($\Delta t_d = \Delta t_c = 1800$ ns) and the working frequency in this PT-symmetric state is $f \approx 71$ kHz, which agrees with the theoretical analysis. Fig. 11a shows the output power of the system. It can be observed that the output power reduces when the system works in either an under-compensated state or a highly over-compensated state. In the under-compensated system, the propagation delay results in high switching loss (see Fig. 12). As a result, in the highly under-compensated region, the efficiency of the system is low (see Fig. 11b). Soft switching can be achieved in the over-compensated system, when the compensation further increases, the efficiency first increases and then decreases (see Fig. 11b). This result is attributed to the fact that over-compensation increases the reactive current of the system, leading to increased conduction loss of the switch and transmission loss of the coils. Therefore, the optimal compensation is a trade-off between the conduction losses and switching losses. The maximum efficiency can be achieved when the system is slightly over-compensated.

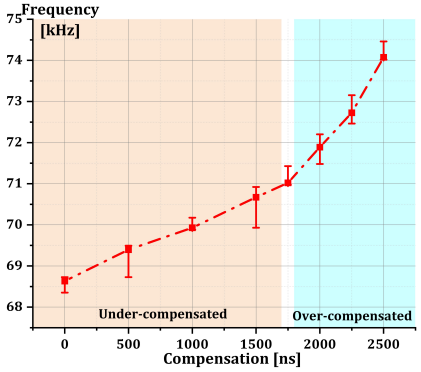

Fig. 10: Experimental result of the system working frequency under different compensation conditions

C. The Steady State Performance Under Different Misalignments

The performance of the system under various misalignment conditions d is investigated with a load resistance $R_L = 10\ \Omega$ and an input voltage of $V_{dc} = 100$ V. The result is shown

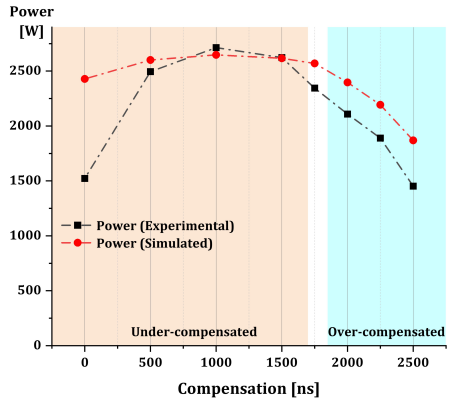

(a) Output power

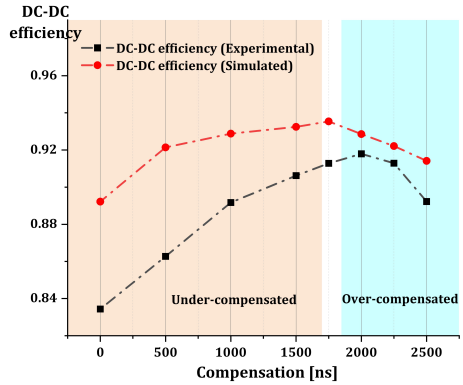

(b) DC-DC efficiency

Fig. 11: Effect of compensation on system efficiency and output power ($V_{dc} = 200$ V, $R_L = 16\ \Omega, k = 0.58$)

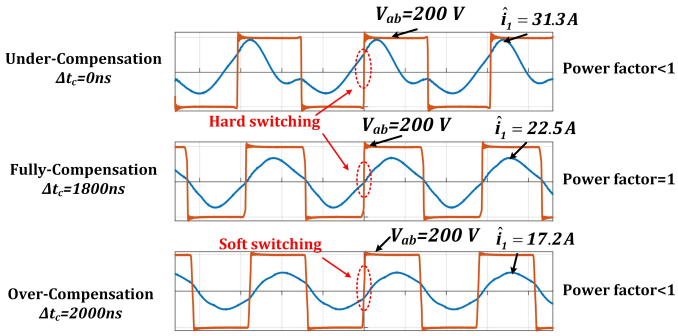

Fig. 12: Experiment waveform with different compensations

in Fig. 13. It can be observed in Fig. 13a that in the fully-compensated condition ($\Delta t_c = 1800$ ns), the system achieves constant output power in the PT-symmetric phase (with misalignment $d \in [0, 160]$ mm), which agrees with the analysis in (6). In the uncompensated case ($\Delta t_c = 0$ ns), variations in output power are observed due to the frequency-dependent characteristic of output power. In both fully-compensated and uncompensated cases, the output power increases with the rise in misalignment in the PT broken phase. As the working frequency is maintained at $f_0 = 83.5$ kHz. The DC-DC efficiency is shown in Fig. 13b. In the PT-symmetric phase, the fully-compensated system has higher efficiency than the uncompensated system. This is attributed to the fact that the uncompensated system has high switching loss due to hard switching and high transmission loss due to reactive current. Therefore, compensation is necessary to achieve high efficiency and constant power output in the PT-symmetric phase.

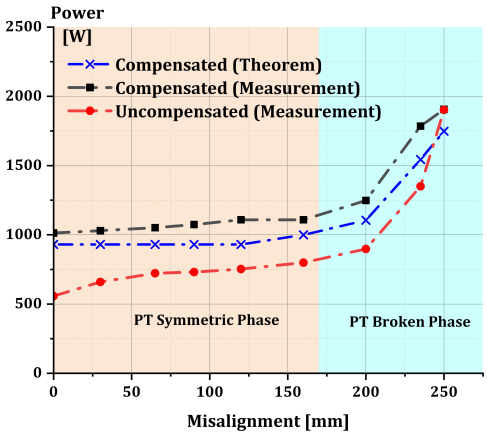

(a) Output power

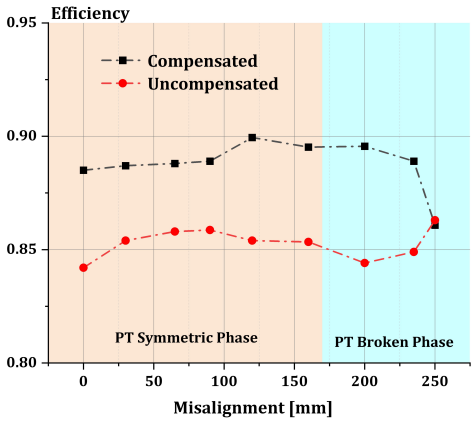

(b) DC-DC efficiency

Fig. 13: Power and efficiency under different misalignment conditions ($V_{dc} = 100$ V, $R_L = 10\ \Omega$)

V. Conclusion

PT-symmetric control scheme provides a promising solution for building high misalignment tolerance IPT system. By synchronizing the inverter output voltage with the transmitter current, constant output power is achieved in the PT-symmetric phase. However, the inherent propagation delay in control circuit can cause frequency drift and high switching loss problem, which reduces the efficiency and output power of the system. To solve this problem, in this article, a digital compensation scheme of the IPT system is proposed. The experimental results shows that the proposed digital control scheme can compensate the delay without

requiring additional compensation circuits. Constant output power is achieved when the delay is fully compensated. Moreover, over-compensation can be employed to realized soft switching, resulting in higher DC-DC efficiency. The proposed control scheme can improve the robustness and efficiency of wireless charging system. The compensation is easy to achieve in hardware experiment and there is no need of high-precision processor.

REFERENCES

[1] A. Ahmad, M. S. Alam, and R. Chabaan, "A Comprehensive Review of Wireless Charging Technologies for Electric Vehicles," *IEEE Transactions on Transportation Electrification*, vol. 4, no. 1, pp. 38–63, 2018.

[2] S. Aldhaher, P. D. Mitcheson, J. M. Arteaga, G. Kkelis, and D. C. Yates, "Light-weight wireless power transfer for mid-air charging of drones," in *2017 11th European Conference on Antennas and Propagation (EUCAP)*, pp. 336–340, 2017.

[3] S. Y. Choi, B. W. Gu, S. Y. Jeong, and C. T. Rim, "Advances in Wireless Power Transfer Systems for Roadway-Powered Electric Vehicles," *IEEE Journal of Emerging and Selected Topics in Power Electronics*, vol. 3, no. 1, pp. 18–36, 2015.

[4] A. Kurs, A. Karalis, R. Moffatt, J. D. Joannopoulos, P. Fisher, and M. Soljačić, "Wireless Power Transfer via Strongly Coupled Magnetic Resonances," *Science*, vol. 317, no. 5834, pp. 83–86, 2007.

[5] F. Z. Shen, W. Z. Cui, W. Ma, J. T. Huangfu, and L. X. Ran, "Circuit analysis of wireless power transfer by "coupled magnetic resonance"," in *IET International Communication Conference on Wireless Mobile and Computing (CCWMC 2009)*, pp. 602–605, 2009.

[6] J. L. Villa, J. Sallan, J. F. Sanz Osorio, and A. Llombart, "High-Misalignment Tolerant Compensation Topology For ICPT Systems," *IEEE Transactions on Industrial Electronics*, vol. 59, no. 2, pp. 945–951, 2012.

[7] J. M. Arteaga, S. Aldhaher, G. Kkelis, C. Kwan, D. C. Yates, and P. D. Mitcheson, "Dynamic Capabilities of Multi-MHz Inductive Power Transfer Systems Demonstrated With Batteryless Drones," *IEEE Trans. Power Electron.*, vol. 34, no. 6, pp. 5093–5104, 2019.

[8] M. Budhia, J. T. Boys, G. A. Covic, and C.-Y. Huang, "Development of a Single-Sided Flux Magnetic Coupler for Electric Vehicle IPT Charging Systems," *IEEE Transactions on Industrial Electronics*, vol. 60, no. 1, pp. 318–328, 2013.

[9] J. Huang, Y. Dou, X. Huang, Z. Zhang, Z. Ouyang, and M. A. Andersen, "Optimization of a 6.78-MHz Inductive Power Transfer System for Unmanned Aerial Vehicles," *IEEE Trans. Power Electron.*, vol. 38, no. 10, pp. 11940–11952, 2023.

[10] H. Sakamoto, K. Harada, S. Washimiya, K. Takehara, Y. Matsuo, and F. Nakao, "Large air-gap coupler for inductive charger [for electric vehicles]," *IEEE Transactions on Magnetics*, vol. 35, no. 5, pp. 3526–3528, 1999.

[11] J. Lei, M. Junaid, D. Yu, Z. Hua, and S. Yu, "A Double-Side Feedback Pulse Train Control for the Output Voltage Regulation of Two-Stage Wireless Power Transfer System," *Applied Sciences*, vol. 12, no. 18, p. 8991, 2022.

[12] J. Liu, K. W. Chan, C. Y. Chung, N. H. L. Chan, M. Liu, and W. Xu, "Single-Stage Wireless-Power-Transfer Resonant Converter With Boost Bridgeless Power-Factor-Correction Rectifier," *IEEE Transactions on Industrial Electronics*, vol. 65, no. 3, pp. 2145–2155, 2018.

[13] Z. Bie, J. Zhang, K. Song, D. Wang, and C. Zhu, "A Free-Rotation Asymmetric Magnetic Coupling Structure of UAV Wireless Charging Platform With Conformal Pickup," *IEEE Transactions on Industrial Electronics*, vol. 69, no. 10, pp. 10154–10161, 2022.

[14] D. Pehrman and Y. Liu, "Design and Stray Field Evaluation of Inductive Power Transfer in Electric Vehicle Charging," in *2019 Fourteenth International Conference on Ecological Vehicles and Renewable Energies (EVER)*, pp. 1–6, 2019.

[15] E. S. Lee, "Frequency-Modulation-Based IPT With Magnetic Communication for EV Wireless Charging," *IEEE Transactions on Industrial Electronics*, vol. 70, no. 2, pp. 1398–1408, 2023.

[16] C. Cui, Y. Liu, D. Pehrman, X. Huang, and Q. Zhang, "A Full Power Range ZVS Control Technology for Bidirectional Inductive Power Transfer System," in *IECON 2020 The 46th Annual Conference of the IEEE Industrial Electronics Society*, pp. 3861–3865, 2020.

[17] D. Pehrman, Y. Liu, C. Cui, and X. Huang, "Loss Reduction by Synchronous Rectification in a 50 kW SiC-based Inductive Power Transfer System," in *IECON 2020 The 46th Annual Conference of the IEEE Industrial Electronics Society*, pp. 3907–3912, 2020.

[18] S. Assawaworrarit, X. Yu, and S. Fan, "Robust wireless power transfer using a nonlinear parity–time-symmetric circuit," *Nature*, vol. 546, no. 7658, pp. 387–390, 2017.

[19] J. Zhou, B. Zhang, W. Xiao, D. Qiu, and Y. Chen, "Nonlinear Parity-Time-Symmetric Model for Constant Efficiency Wireless Power Transfer: Application to a Drone-in-Flight Wireless Charging Platform," *IEEE Transactions on Industrial Electronics*, vol. 66, no. 5, pp. 4097–4107, 2019.

[20] L. Wu, B. Zhang, and Y. Jiang, "Position-Independent Constant Current or Constant Voltage Wireless Electric Vehicles Charging System Without Dual-Side Communication and DC–DC Converter," *IEEE Transactions on Industrial Electronics*, vol. 69, no. 8, pp. 7930–7939, 2022.

[21] R. Okada, R. Ota, and N. Hoshi, "Novel Soft-Switching Active-Bridge Converter for Bi-directional Inductive Power Transfer System," *IEEJ Journal IA*, vol. 11, no. 1, pp. 97–107, 2022.

[22] R. Ota, D. J. Thrimawithana, U. K. Madawala, and G. A. Covic, "Boundary of Soft-switching for Efficient Operation of Bi-directional IPT Systems," in *2020 IEEE PELS Workshop on Emerging Technologies: Wireless Power Transfer (WoW)*, pp. 164–169, 2020.